Experimental Characterization of Indoor Multi-Link Channels

Claude Oestges[1], Nicolai Czink[2,3], Bernd Bandemer[3], Paolo Castiglione[2], Florian Kaltenberger[4] and Arogyaswami Paulraj[3]

[1]Microwave Laboratory, Université catholique de Louvain, Louvain-la-Neuve, Belgium
[2]Forschungszentrum Telekommunikation Wien (ftw.), Vienna, Austria
[3]Smart Antennas Research Group, Stanford University, Stanford, CA, USA
[4]Mobile Communications Department, Eurecom Institute, Sophia-Antipolis, France

***Abstract*—In this paper, an empirical model of the indoor distributed channel is presented. In particular, the shadowing and fading statistics are extracted from experimental data at 2.45 GHz in stationary and mobile scenarios. Highlights of the paper include a separate model for static and dynamic shadowing, a model for shadowing correlation, as well as a single analytical distribution of small-scale fading for various types of indoor node mobility.**

I. Introduction

An alternative to the installation of additional base stations to increase indoor radio coverage is to establish collaboratively a reliable wireless link between a set of indoor nodes to a base station not necessarily in reach of the individual nodes. Yet, before developing algorithms tackling this challenge, the multi-link channel between all indoor nodes must be measured and modeled. The current paper proposes an empirical model of the indoor distributed channel for stationary and mobile indoor nodes. In previous works [1, 2], various properties of indoor distributed channels have been analyzed for stationary nodes only. Fading was modeled in [1] by a generalized gamma distribution, which might not be easily tractable. Mobile multi-link measurements were presented in [3], for indoor MIMO channels with two base stations and two users, and in [4] for outdoor channels. Our analysis, focused on indoor distributed (or multi-link) channels, includes both stationary and mobile scenarios and provides an accurate and low-complexity model for the small-scale fading distribution with a direct physical interpretation [5]. Furthermore, we model shadowing correlation, which was measured and characterized in [6] for non-distributed indoor channels and in [2] for sensor networks, but without taking into account the impact of node mobility. By contrast, the parameters of our model are related to the mobility scenario (i.e. the number of moving nodes).

This work was partially supported by the European Commission in the framework of the FP7 Network of Excellence in Wireless COMmunications NEWCOM++ (contract no. 216715), by US Army grant W911NF-07-2-0027-1, and by the Vienna Science and Technology Fund in the ftw. project PUCCO. It was also carried out in cooperation within the European COST 2100 Action. The Telecommunications Research Center Vienna (ftw.) is supported by the Austrian Government and the City of Vienna within the competence center program COMET. The work of C. Oestges is supported by the Belgian Fonds de la Recherche Scientifique (FRS-FNRS). The work of N. Czink is supported by an Erwin Schroedinger Fellowship of the Austrian Science Fund (FWF grant number J2789-N14). The work of B. Bandemer is supported by an Eric and Illeana Benhamou Stanford Graduate Fellowship. The work of P. Castiglione is supported by the Austria Science Fund (FWF) through grant NFN SISE (S106). The work of F. Kaltenberger is supported by the European Commission in the framework of the FP7 project SENDORA (contract no. 216076) and by Eurecom.

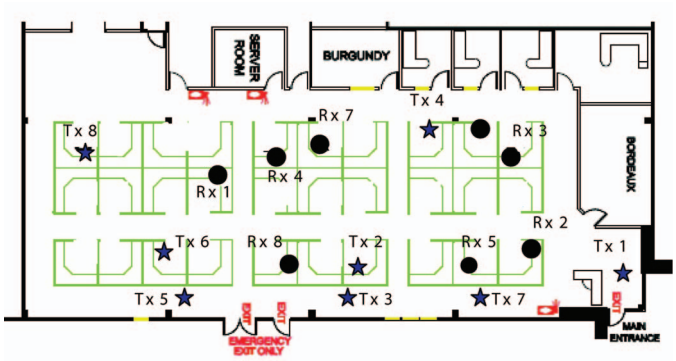

Fig. 1. Experimental set-up

II. Experimental Set-Up

This paper is based on channel measurements from the Stanford July 2008 Radio Channel Measurement Campaign. In this section, we briefly summarize the most important characteristics of the measurement set-up.

A. Environments

The terminals were located in a typical U.S. office environment, and used two different kinds of off-the-shelf vertically polarized WiFi antennas matched at 2.45 GHz. Their gain is 7dBi and 10dBi, respectively, specified in the range of 2.4-2.83 GHz. The 8 receive locations are represented by the circles in Figure 1, while the 8 Tx locations are represented by the stars. Three types of measured scenarios are investigated: (i) stationary measurements, where slow fading was generated by walking people carrying metallic objects, (ii) time-variant measurements, where all 8 receive antennas were moved randomly within a 2 m radius (inside a cubicle); (iii) time-variant measurements, where 4 of the Tx antennas and 4 of the Rx antennas were moved randomly within a 2 m radius (inside a cubicle). Each of these scenarios was measured twice to allow for excluding measurement artifacts.

B. Measurement Equipment

The measurements were taken using the RUSK Stanford channel sounder at a center frequency of 2.45 GHz with a bandwidth of 240 MHz, and a test signal length of 3.2 μs. Owing to occasional interference (e.g. from WiFi equipments and microwave ovens), the channel characterization is carried out over the lowest 70 MHz of the measured spectrum, i.e. the band from 2.33 to 2.40 GHz. Additionally, several frequencies have been removed (approximately every 10 MHz) to avoid antenna effects. Since all evaluations were done in the frequency domain only, the cutting of frequencies does not have any impact on the results. The transmitter output power of the sounder was 0.5 W. A rubidium reference in the transmit (Tx) and receive (Rx) units ensured accurate timing and clock synchronization. The sounder used fast 1×8 switches at both transmitter and receiver, enabling switched-array MIMO channel measurements of up to 8×8 antennas, i.e. 64 links. One measurement of the whole MIMO channel at one time instant is denoted as a *block*. The recorded frequency responses of the MIMO channels are organized in a multi-dimensional array $H[t, f, n, m]$, with dimensions time (in blocks), frequency tone, receivers, and transmitters. For the stationary case, the number of blocks recorded (T) was equal to 120, each block being separated by 250 ms. In the mobile cases, 1200 blocks spaced by 9.83 ms were measured. Finally, since two types of WiFi antennas were used, an antenna gain correction was implemented in the post-processing to compensate for the gain difference.

III. General Concepts of Data Analysis

Throughout this paper, the channel coefficients are considered to reflect the superposition of the following propagation effects:

$$\begin{aligned}\text{channel } &= \text{path loss } \times \text{ static shadowing } \times \\ &\times \text{ dynamic shadowing} \times \text{fading}\end{aligned}$$

The *path-loss* denoted as Λ in dB scale is defined as the deterministic distance dependence of the received power. Shadowing, denoted as S in dB scale, is caused by obstruction of the link, and results in the individual path loss to vary with location and time. In the representation above, shadowing is expressed by the multiplication of two terms, i.e. static and dynamic shadowing (this multiplication is equivalent to adding the dB levels). *Static shadowing*, denoted as $\bar{S}$ [dB], is the time-invariant mean shadowing (when expressed in dB) and the difference between the time-averaged received powers of two links sharing the same range. It is therefore linked to time-invariant obstructions of the link, which can of course differ for each node. For stationary scenarios, static shadowing also results from the constructive or destructive combination of coherent multipaths, which, for a given link, causes static shadowing to possibly vary with frequency. *Dynamic shadowing*, represented by the variable $\tilde{S}$ [dB], is the slow temporal variation of the received power around its mean. It is caused by the mobility of either scatterers such as people, or the stations themselves moving throughout the environment. Finally, *fading*, denoted as r, is the classical small-scale fading behavior of the channel caused by the small-scale motions of the stations and/or the environment. The distinction between dynamic shadowing and fading is therefore the temporal scale of the channel variations. For a given link, the instantaneous received power at time t is therefore proportional to $|r(t)|_{\text{dB}} - \Lambda - \bar{S} - \tilde{S}(t)$, where the operator $|_{\text{dB}}$ denotes the conversion to dB. The individual path loss L of each link is defined as the total time-invariant path-loss, i.e. $L = \Lambda + \bar{S}$.

IV. Parameter Estimation

A. Data Preprocessing

The whole frequency band is first partitioned into subbands of F_{sub} frequency tones each, leading to a total number of $B = F/F_{\text{sub}}$ subbands per time instant and link. Using subbands to increase the sample size is feasible for the stationary measurements, since the coherence bandwidth is low. In this case, we chose $F_{\text{sub}} = 5$. However, for moving measurements, the coherence bandwidth appears to be very large, hence it is not necessary to divide the whole frequency band, which is then considered as a single subband (i.e. $F_{\text{sub}} = F$).

B. Path Loss and Static Shadowing

Let us consider the link between transmitter m and receiver n. We denote by $d = d_{nm}$ the distance between these nodes. The average received power in the b^{th} subband is then obtained by averaging the power within the subband and over all time samples,

$$P[b, n, m] = \frac{1}{F_{\text{sub}} T} \sum_{t=1}^{T} \sum_{f=1+(b-1)F_{\text{sub}}}^{bF_{\text{sub}}} |H[t, f, n, m]|^2, \quad (1)$$

with $b = 1 \ldots B,\ n = 1 \ldots 8,\ m = 1 \ldots 8$ (remember that there is only one subband in the moving case, equal to the whole 70 MHz bandwidth). We model path-loss and static shadowing by expressing the received power as

$$P|_{\text{dB}}(d) = P_0|_{\text{dB}} - \eta \cdot 10 \log_{10}\left(\frac{d}{d_0}\right) - \bar{S}, \quad (2)$$

where $P|_{\text{dB}}$ denotes the observed received power for a distance d between transmitter and receiver, P_0 and d_0 denote the reference power and reference distance, respectively. The static shadowing $\bar{S}$, which differs in each subband in the stationary case (this is not the case in the moving scenarios, which is why the full bandwidth is considered as a single subband), is then defined as the difference between the observed power and the deterministic received power. It is a time-invariant random variable for each link and each considered subband. It is classically assumed to be a zero-mean Gaussian variable (i.e. lognormal in natural scale), characterized by its standard deviation $\sigma_{\bar{S}}$.

C. Dynamic Shadowing

Analogous to static shadowing, the time-variant dynamic shadowing can differ significantly in the different subbands

when considering stationary scenarios. For this reason, $\tilde{S}$ is also estimated for the B subbands individually. We first average the received power over each subband for each time instant and link. Subsequently, we further average over the small-scale fading by using a moving window spanning $T_{\text{av}} = 2.6\,s$ (corresponding to either 10 samples for the stationary measurements or 160 samples for the moving measurements),

$$P_s[t,b,n,m] = \frac{1}{F_{\text{sub}}T_{\text{av}}} \sum_{t'=t-T_{\text{av}}/2}^{t+T_{\text{av}}/2-1} \sum_{f=1+(b-1)F_{\text{sub}}}^{bF_{\text{sub}}} |H[t',f,n,m]|^2 . \quad (3)$$

Finally, we obtain $\tilde{S}[t,b,n,m]$ as the variation of $P_s|_{\text{dB}}$ around its mean,

$$\tilde{S} = P_s|_{\text{dB}} - \mathrm{E}_t\{P_s|_{\text{dB}}\}, \quad (4)$$

where $\mathrm{E}_t\{\cdot\}$ denotes the sample mean over the time axis, and the $[t,b,n,m]$ dependence is dropped to simplify the notations. Dynamic shadowing is usually assumed to be log-normal distributed [7], i.e. $\tilde{S}$ is Gaussian distributed, with a mean $\mu_{\tilde{S}} = 0$ by definition, the standard deviation $\sigma_{\tilde{S}}$ being the model parameter. The latter was estimated using the sample variance [8]. Since $\tilde{S}$ may be correlated between different links (n,m) and (n',m'), we calculated the correlation coefficient between $\tilde{S}[t,b,n,m]$ and $\tilde{S}[t,b,n',m']$. These correlation coefficients are evaluated between all 64 links in one measurement and are grouped in different sets: links with a common Rx (denoted as 'Rx'), with a common Tx (denoted as 'Tx'), with a common Rx or a common Tx (union of sets 1 and 2, denoted as 'Rx-Tx'), with no node in common (complement of set 3, denoted as 'disjoint'), and all links (union of sets 3 and 4, denoted as 'all').

D. Fading

Small-scale fading is described by the statistics of the received signal amplitude, r. Before estimating the different kinds of fading, we remove the effects of path-loss and shadow fading by normalizing each channel by its respective power as

$$G[t,f,n,m] = \frac{H[t,f,n,m]}{\sqrt{P_s[t,\lceil f/F_{\text{sub}}\rceil,n,m]}}, \quad (5)$$

where $\lceil\cdot\rceil$ is the ceiling function. The signal amplitude is then simply defined as $r = |G|$. To estimate the statistics of r, we use as ensembles the data from all tones in each subband, and all time samples. For the stationary scenarios, we have therefore model parameter estimates for each of the considered subbands. In the following, we discuss three different types of fading and present their parameter estimators.

1) Ricean fading: We adopt the formulation of the Ricean distribution from [9] as

$$p_{\text{Rice}}(r) = \frac{r}{\sigma^2}\mathrm{e}^{-\left(\frac{r^2}{2\sigma^2}+K\right)}\mathrm{I}_0\left(r\frac{\sqrt{2K}}{\sigma}\right), \quad (6)$$

where $\mathrm{I}_0(\cdot)$ denotes the modified Bessel function of the first kind and zero-th order, $2\sigma^2$ denotes the average power of the non-coherent part, and the K-factor describes the ratio between the powers of the coherent part and the non-coherent part of the channel. Both K and σ^2 are estimated by numerical curve fitting.

2) Rayleigh/Double-Rayleigh fading: The Ricean fading distribution includes pure Rayleigh fading as the limiting case for $K = 0$. In some measured scenarios, however, we observe fading that is more severe than Rayleigh fading. To model this effect, we assume that the channel can be expressed as $G = w_1G_1 + w_2G_2G_3$, where G_1, G_2, G_3 are i.i.d. complex normal random variables with zero mean and unit variance. The two terms can be interpreted as a single-bounce Rayleigh-fading component and a two-bounce Double-Rayleigh-fading component, respectively. Under this model, the probability density function of $r = |G|$ is (see, for example [5])

$$p_{\text{RDR}}(r) = r\int_0^\infty \mathrm{e}^{-\frac{w_1^2\omega^2}{4}}\frac{4\omega}{4+w_2^2\omega^2}\,\mathrm{J}_0(r\omega)\,\mathrm{d}\omega,$$

where J_0 is the Bessel function of the first kind and zero-th order. We call this the RDR distribution. The distribution parameters w_1 and w_2 can be estimated based on the method of moments and refined by curve fitting, also noting that the relationship $\mathrm{E}_t\{r^2\} = 1$ is achieved when $w_1^2 + w_2^2 = 1$. To characterize the trade-off between Rayleigh and Double-Rayleigh fading explicitly, we define $\alpha = w_2^2/(w_1^2 + w_2^2)$, so that $\alpha = 1$ is equivalent to Double-Rayleigh fading, while $\alpha = 0$ denotes pure Rayleigh fading.

3) Nakagami fading: The Nakagami-*m* distribution is given by [7]:

$$p_{\text{Naka}}(r) = \frac{2}{\Gamma(m)}\left(\frac{m}{\Omega}\right)^m r^{2m-1}\mathrm{e}^{-mr^2/\Omega}, \quad (7)$$

where Ω is the second moment, $\Gamma(\cdot)$ denotes the Gamma function and the m-parameter (sometimes denoted as shape parameter) is defined as $m = \Omega^2/\mathrm{E}\left\{\left(r^2-\Omega\right)^2\right\}$, $m \geq 0.5$, and can be estimated by the approximation of the maximum-likelihood estimator proposed in [10]. Note that $\Omega = 1$ if $\mathrm{E}_t\{r^2\} = 1$.

While the Nakagami distribution is mathematically tractable for analytical investigations, it has a number of shortcomings: (i) in contrast to the Ricean and Rayleigh/Double-Rayleigh distributions, it has no physical interpretation, (ii) for this reason, it does not fit the measurements as well, (iii) there is no analytical random-number generator for this distribution (only slow, iterative methods exist).

V. Channel Characterization

A. Stationary Nodes

If not indicated differently, the channel parameters were extracted from the distributed-nodes environment shown in Fig. 1, for all channels between the 8 transmitters and 8 receivers. The parameter estimation was carried out as described in Section IV.

1) Path loss and static shadowing: We evaluated the relative path loss as a function of the Tx-Rx distance from the

TABLE I
SHADOWING CORRELATION

Scenario	Subset	Mean	Std.	Max	Min
Static	all	0.00	0.27	0.94	-0.90
Single mobile (Rx)	all	0.05	0.38	0.99	-0.91
	Rx	0.47	0.41	0.99	-0.79
	Tx	-0.01	0.35	0.80	-0.83
	Rx-Tx	0.23	0.45	0.99	-0.83
	disjoint	0.00	0.34	0.90	-0.91
Single mobile (Tx)	all	0.05	0.41	0.99	-0.93
	Rx	0.00	0.36	0.81	-0.82
	Tx	0.37	0.50	0.99	-0.84
	Rx-Tx	0.19	0.47	0.99	-0.84
	disjoint	0.01	0.37	0.87	-0.93
Double mobile	all	0.16	0.39	0.97	-0.90
	Rx	0.29	0.36	0.89	-0.40
	Tx	0.29	0.42	0.97	-0.74
	Rx-Tx	0.29	0.39	0.97	-0.74
	disjoint	0.06	0.36	0.81	-0.90

data and extract the path-loss model as

$$L = L_0 + 1.75 \cdot 10 \log_{10}\left(\frac{d}{d_0}\right) + \bar{S}, \tag{8}$$

where $d_0 = 1$ m, L_0 is defined as the reference path loss in the absence of obstruction at a distance d_0 =1 m, and the static shadowing $\bar{S}$ is a zero-mean Gaussian distributed variable over space, with a standard deviation $\sigma_{\bar{S}} = 5.85$ dB. Interestingly, the value of $\eta = 1.75$ is smaller than 2, which tends to indicate that waveguiding propagation effects take place.

2) Dynamic shadowing: For the *standard deviation of dynamic shadowing*, we observed that is strongly correlated with the individual path loss and the distance. Hence, it is modeled as

$$\log_{10}(\sigma_{\tilde{S}}) = \log_{10}(\sigma_{\tilde{S},0}) + 0.02(L - L_0) + \sigma_{\sigma_{\tilde{S}}}, \tag{9}$$

versus path loss and as

$$\log_{10}(\sigma_{\tilde{S}}) = \log_{10}(1.85) + 0.2 \log_{10}\left(\frac{d}{d_0}\right) + \sigma'_{\sigma_{\tilde{S}}}, \tag{10}$$

versus distance with $\sigma_{\sigma_{\tilde{S}}}$ and $\sigma'_{\sigma_{\tilde{S}}}$ being zero-mean Gaussian distributed, with a standard deviation of 0.16 and 1.13 respectively. Regarding the dynamic shadowing correlation, it was found that all sets ('Rx', 'Tx', 'Rx-Tx' and 'disjoint') showed a very similar behavior in terms of mean, standard deviation and extrema, and no clear relationship with the geometry of the links could be established. Hence, in Table I, only the results of the 'all' set are provided.

3) Fading: For stationary antennas, the normalized channel gain is naturally found to be Ricean distributed, with the K-factor closely related to the to the Tx-Rx distance (resembling the global path loss), but also to the individual path loss, as illustrated in Fig. 2. These trends can be fitted by the following laws:

$$K|_{\text{dB}} = 16.90 - 5.25 \log_{10}\left(\frac{d}{d_0}\right) + \sigma'_K, \tag{11}$$

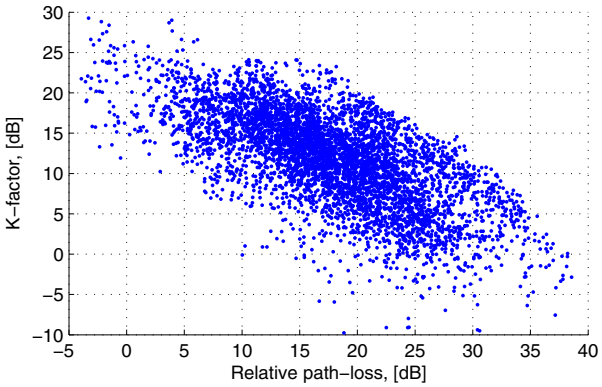

Fig. 2. K-factor vs. relative path loss for the stationary data

where d is the Tx-Rx distance in meters, $d_0 = 1$ m and σ'_K is approximately a random Gaussian variable of deviation standard equal to 6 dB, and

$$K|_{\text{dB}} = K_0|_{\text{dB}} - 0.57\,(L - L_0) + \sigma_K, \tag{12}$$

where σ_K is a random Gaussian variable of standard deviation equal to 4.6 dB. Similar trends are found for the Nakagami m-parameter, which is fitted by

$$\log_{10}(m) = 1.35 - 0.50 \log_{10}\left(\frac{d}{d_0}\right) + \sigma'_m \tag{13}$$

over distance, and by

$$\log_{10}(m) = \log_{10}(m_0) - 0.053(L - L_0) + \sigma_m \tag{14}$$

over the individual relative path loss. Variables σ'_m and σ_m are Gaussian distributed with standard deviations equal to 0.48 and 0.38, respectively. Both distributions are truncated so that $m > 0.5$.

B. Mobile Nodes

1) Path loss and static shadowing: It was found that both the path loss coefficient and the static shadowing standard deviation are similar to the stationary-node case.

2) Dynamic shadowing: In contrast to the stationary case, the *standard deviation of dynamic shadowing*, $\sigma_{\tilde{S}}$, does not depend on the path loss any more when one or both stations are moving, but it is rather constant. We observed it to be similar to the static shadowing, hence we model $\sigma_{\tilde{S}} = \sigma_{\bar{S}}$. Table I also provides the results on the correlation coefficients. In the table, we distinguish two types of mobility: (i) either only one node (Tx or Rx) is moving (*single-mobile*), or (ii) both nodes (Tx and Rx) are moving (*double-mobile*). It can be seen that in all cases, the sets for which at least one moving node (Tx or Rx) is common to both links, clearly show a higher correlation than the sets for which the moving node is not common: for the single-mobile case with moving Rx, the 'Rx' set shows a higher correlation than the 'Tx' set, while the opposite is observed for the the single-mobile case with moving Tx; for the double-mobile case, all sets containing a joint moving node show similar values, by contrast to the 'disjoint' set.

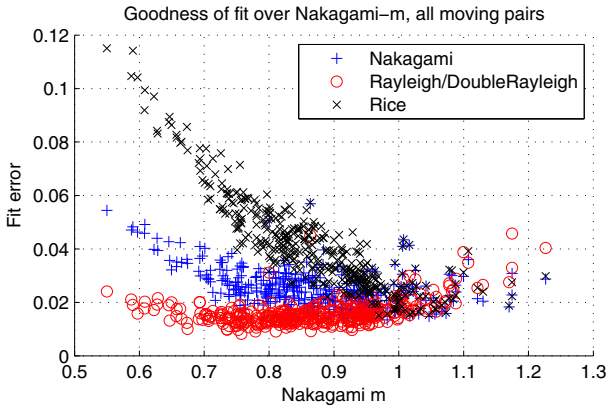

Fig. 3. Goodness of fit of all considered PDFs vs. m-parameter.

3) Fading: We find that the small-scale fading statistics for this scenario vary between pure Rayleigh fading and worse-than-Rayleigh fading, i.e., fading in which smaller amplitudes are more probable than in the Rayleigh distribution. As outlined in Section IV-D, a smooth transition between Rayleigh and below-Rayleigh distributions can be modeled by both the Nakagami distribution p_{Naka} (with $0.5 < m < 1$) and the RDR distribution p_{RDR}. For reference purposes, the Rice distribution p_{Rice} was also fitted to the data. The fitting is implemented using standard non-linear minimization algorithms, where the L_∞ norm of the CDF deviation plays the role of a goodness of fit measure (the smaller the norm, the better the fit). In Fig. 3, the goodness of fit for the three distributions are compared to each other for all links where at least one node is moving. For $m < 1$, RDR generally achieves a better distribution fit than Nakagami. For $m > 1$, not surprisingly, RDR performs slightly worse than Nakagami or Rice.

Therefore, the fading process can be modeled in two parts: some links fade worse than Rayleigh and can be modeled by the RDR distribution, and some links fade above or equal to Rayleigh and can be modeled by the Ricean distribution. Since there is no discernible correlation between the fading parameters and the distance, we take on a stochastic approach, and distinguish again between *single-mobile* and *double-mobile* cases. We conclude from the data that for double-mobile links, roughly 96.9% experience fading worse than Rayleigh fading, while for single-mobile links, this percentage falls to 90.9%. The remaining links experience fading above or equal to the Rayleigh distribution. Given the small percentage of these links, and the fact that their K-factors are low, they can approximately also be modeled by the RDR distribution with $\alpha = 0$. The data analysis suggests that a (truncated) normal distribution adequately captures the behavior of α in both cases, approximately with the same standard deviation, but with the mean value of α significantly higher when both nodes are mobile, so that the global distribution of α is given for single-mobile links by

$$\alpha \sim 0.091 \cdot \delta + 0.909 \cdot \mathcal{N}_{]0,1[}(0.39, 0.13), \qquad (15)$$

and for double-mobile links by

$$\alpha \sim 0.031 \cdot \delta + 0.969 \cdot \mathcal{N}_{]0,1[}(0.54, 0.12), \qquad (16)$$

where δ is the PDF of a random variable that is always 0, and $\mathcal{N}_{]0,1[}(\mu, \sigma)$ is a Gaussian variable of mean μ and standard deviation σ truncated in $]\,0, 1\,[$.

VI. Conclusions

This paper presented the analysis and modeling of the indoor multi-link channel based on experimental results. A statistical model of stationary and mobile channels was proposed, with a physically-motivated separation of static shadowing (caused by time-invariant obstructions) and dynamic shadowing (caused by mobility of nodes and/or obstacles), each effect being described as a lognormal variable. The standard deviation of static (in all cases) and dynamic shadowing (in mobile cases) is about 5.85 dB. For stationary cases, the standard deviation of dynamic shadowing is correlated with the relative path loss. We also proposed an analysis of the dynamic shadowing correlation, in order to relate the correlation to the node mobility. Small-scale fading is well approximated by a Ricean or an m-Nakagami distribution, the parameters of which being closely related to path loss or the distance for stationary cases, whereas for mobile nodes, it is modeled by a single distribution, consisting of a combination of Rayleigh and Double-Rayleigh fading. We found that the distribution is more tilted toward Double-Rayleigh when both Tx and Rx nodes are moving. Future work will consist in (i) extending the small-scale fading model to better represent Ricean channels, (ii) considering the corresponding outdoor-to-indoor (O2I) channel, and (iii) proposing a complete statistical model for both links [11].

References

[1] J. Karedal, A. Johansson, F. Tufvesson, and A. Molisch, "A measurement-based fading model for wireless personal area networks," *IEEE Trans. Wireless Commun.*, vol. 7, no. 11, pp. 4575–4585, Nov. 2008.

[2] P. Agrawal and N. Patwari, "Correlated link shadow fading in multi-hop wireless networks," Tech. Rep. arXiv:0804.2708, Apr 2008. [Online]. Available: http://arxiv.org/abs/0804.2708

[3] P. Almers, K. Haneda, J. Koivunen, V.-M. Kolmonen, A. F. Molisch, A. Richter, J. Salmi, F. Tufvesson, and P. Vainikainen, "A dynamic multi-link mimo measurement system for 5.3 ghz," in *Proc. The 29th URSI General Assembly*, Chicago, USA, Aug. 2008.

[4] F. Kaltenberger, M. Kountouris, D. Gesbert, and R. Knopp, "Correlation and capacity of measured multi-user MIMO channels," in *Proc. IEEE Intl. Symposium on Personal, Indoor and Mobile Radio Communications (PIMRC)*, Cannes, France, Sep. 2008.

[5] J. Salo, H. M. El-Sallabi, and P. Vainikainen, "Statistical analysis of the multiple scattering radio channel," *IEEE Trans. Antennas Propagat.*, vol. 54, no. 11, pp. 3114–3124, Nov. 2006.

[6] N. Jalden, P. Zetterberg, B. Ottersten, H. Aihua, and R. Thoma, "Correlation properties of large scale fading based on indoor measurements," in *Proc. IEEE Wireless Communications and Networking Conference, WCNC 2007*, Mar. 2007, pp. 1894–1899.

[7] J. Parsons, *The mobile radio propagation channel*. London, UK: 2nd ed., Wiley, 2000.

[8] S. M. Kay, *Fundamentals of Statistical Signal Processing, Estimation Theory*. Prentice Hall, 1993.

[9] C. Oestges and B. Clerckx, *MIMO Wireless Communications*. Elsevier Academic Press, 2007.

[10] J. Cheng and N. N. Beaulieu, "Maximum-likelihood based estimation of the Nakagami m parameter," *IEEE Commun. Lett.*, vol. 5, no. 3, pp. 101–103, Mar. 2001.

[11] C. Oestges, N. Czink, B. Bandemer, P. Castiglione, F. Kaltenberger, and A. Paulraj, "Experimental characterization and modeling of outdoor-to-indoor and indoor-to-indoor distributed channels," in preparation.